Studying Chaos via 1-D Maps—A Tutorial

Chai Wah Wu, *Student Member, IEEE*, and Nikolai F. Rul'kov

***Abstract*— In this introductory tutorial paper, we show how 1-D maps can be useful in analyzing experimentally the chaotic dynamics and bifurcations of circuits and systems. We illustrate this by means of Chua's circuit.**

I. Introduction

ONE OF THE WAYS to make a complex system easier to analyze is by reducing the system to a simpler system that still captures the important features of the original system. For example, in a continuous-time dynamical system, a Poincaré map (also called a first-return map) living in a lower dimensional manifold can provide much insight to the system. In other words, a lower dimensional *discrete-time* dynamical system is constructed from the original system. As the theory of one-dimensional (1-D) maps is well developed, it will be useful if an appropriate 1-D map can be constructed from the system under study. In this tutorial paper, we demonstrate how an approximate 1-D map can be used to analyze the complex dynamics and bifurcation phenomena of the 3-D Chua's circuit, which is described by a system of ordinary differential equations (state equations). In Section II we use the logistic map as an example of a 1-D map and show the complicated dynamics that it possesses. In Section III we illustrate how maps can be constructed from some systems of ordinary differential equations (ODE), in particular, on how a 1-D map can be generated from Chua's circuit. In Section IV we give an experimental analysis of the complex dynamics in Chua's circuit by means of 1-D maps. In Section V we discuss briefly other numerical and theoretical works done on 1-D maps related to Chua's circuit.

II. Example of 1-D Map: The Logistic Map

A simple and well-studied example of a 1-D map that exhibits complicated behavior is the logistic map from the unit interval $[0, 1]$ into $[0, 1]$, parameterized by μ:

$$f_\mu(x) = \mu x(1 - x) \tag{1}$$

where $0 \leq \mu \leq 4$. This map constitutes a discrete-time (semi)dynamical system in the sense that the map f_μ: $[0, 1] \rightarrow [0, 1]$ generates a semigroup through the operation of composition of functions. The state evolution is described by $x_{n+1} = f_\mu(x_n)$. We denote

$$f^{(n)} = \underbrace{f \circ f \circ \cdots \circ f}_{n \text{ times}}.$$

For all $x \in [0, 1]$, we can generate a "discrete-time" trajectory $\{x_i\}_{i=0}^{\infty}$, where $x_i = f^{(i)}(x)$. The set of points $\{x_0, x_1, \cdots\} \subset [0, 1]$ is called the (forward) orbit of x. A *periodic point* of f is a point $x \in [0, 1]$ such that $x = f^{(n)}(x)$ for some positive integer n. The least positive integer n such that this occurs is called the *period* of x. A periodic point of period 1 is called a *fixed point*. If a point is a periodic point of f of period n, then it is the fixed point of $f^{(n)}$. If x is a fixed point of $f^{(n)}$, then it is a periodic point of f whose period divides n. For differentiable f, a periodic point x with period n is stable if

$$\left|\prod_{i=1}^{n} f'(x_i)\right| < 1$$

and unstable if

$$\left|\prod_{i=1}^{n} f'(x_i)\right| > 1$$

where $x_i = f^{(i)}(x)$. If x is a periodic point of period n, then so is $f(x)$. For each fixed μ, the map f_μ can possess stable or unstable periodic points and chaotic attractors, among others. As the parameter μ is varied, changes in the *qualitative* behavior of the system, also called *bifurcations*, can occur.

In the logistic map, as μ is varied from 0 to 4, a period-doubling bifurcation occurs. In the region $\mu \in [0, 3]$, the map f_μ possesses one stable fixed point. As μ is increased past 3, the stable fixed point becomes unstable, and two new stable periodic points are created of period 2. As μ is further increased, these stable periodic points in turn become unstable, each spawning two new stable periodic points of period 4.[1] Thus the period of the stable periodic points is doubled at each bifurcation point. Each period-doubling episode occurs in a shorter "parameter" interval each time, decreasing at a geometric rate, converging at a finite μ to an infinite number of period-doublings at which point chaos is observed. This is depicted in the bifurcation diagram in Fig. 1, where the bifurcation parameter μ is plotted on the horizontal axis, and the attractor(s) of the map is plotted on the vertical axis. Since there is at most one periodic attractor in the logistic map [1], we can show the attractor by plotting the trajectory of an initial

Manuscript received March 20, 1993; revised May 30, 1993. This work was supported by the National Science Foundation under grant MIP 86-14000. This paper was recommended by Guest Editor L. O. Chua.

C. W. Wu is with the Electronics Research Laboratory and the Department of Electrical Engineering and Computer Sciences, University of California, Berkeley, CA 94720.

N. F. Rul'kov is with the Electronics Research Laboratory and the Department of Electrical Engineering and Computer Sciences, University of California, Berkeley, CA 94720. He is on leave from the Radio Physics Department, Nizhny Novgorod State University, Nizhny Novgorod, Russia.

IEEE Log Number 9211610.

[1] Note that all the periodic points on the same orbit becomes unstable at the same parameter value due to the chain rule.

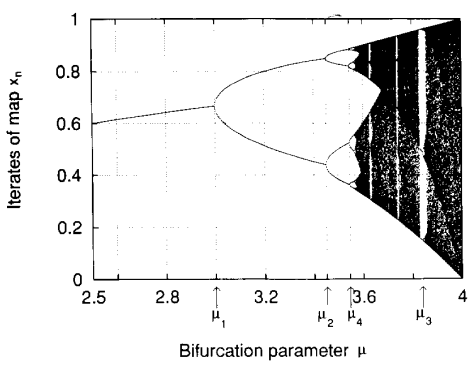

Fig. 1. Bifurcation diagram of the logistic map $f_\mu(x) = \mu x(1-x)$.

point after a large number of transient iterations. This is the algorithm used to generate Fig. 1. The first few bifurcation points μ_n where the n-periodic stable periodic points lose stability and $2n$-periodic stable periodic points emerge are shown in the figure. For maps with a quadratic extremum, as in the case with the logistic map, the nth bifurcation point occurs at successive intervals asymptotically proportional to δ^n, where $\delta \approx 4.669$. In other words,

$$\lim_{n\to\infty} \frac{\mu_{2^{n+1}} - \mu_{2^n}}{\mu_{2^{n+2}} - \mu_{2^{n+1}}} = \delta.$$

As μ is further increased, there is a region of parameter space where a stable period-3 periodic point exists (μ_3 in Fig. 1), which undergoes a period-doubling bifurcation as μ is increased. An interesting theorem of Sarkovskii says that for a continuous 1-D map on the real line, the existence of a period-3 periodic point implies the existence of periodic points of any period [1]. In the logistic map at the parameter μ_3, all other periodic points are unstable, so that most initial conditions will converge towards the stable period-3 periodic point. We will see later that this region of parameter space around μ_3 contains very interesting phenomena such as *intermittency* and *crisis*.

III. Generating Maps from ODE's

From a system of n ordinary differential equations we can obtain a Poincaré map (or first return map) from $\mathbb{R}^{n-1}$ into $\mathbb{R}^{n-1}$ as follows: First, an $(n-1)$-D hyperplane is chosen. Given a point on this hyperplane, the Poincaré map maps this point to the next point on the trajectory through this point which intersects this hyperplane in the same direction.[2] The orbit of the Poincaré map can be thought of as the intersection between the intersecting plane and the trajectory. For a periodic trajectory which is *transversal* to the hyperplane[3] this map is well defined locally around the intersection of the trajectory and the hyperplane. For example, in Fig. 2, we show a periodic orbit intersecting a hyperplane transversally. The point x_1 is mapped by the Poincaré map to x_2 and vice versa. In Chua's circuit, shown in Fig. 3, which is a 3-D system, the corresponding Poincaré map will be a 2-D map.

[2] This is called the *one-sided* Poincaré map in [2].

[3] A plane and a curve intersect transversally in $\mathbb{R}^3$ if and only if the curve crosses the plane non-tangentially [3].

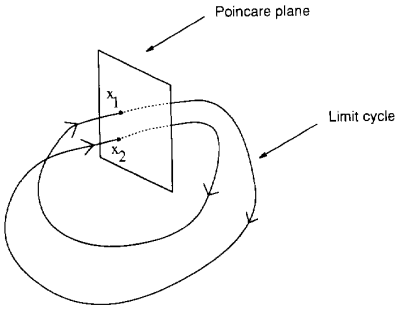

Fig. 2. Poincaré map generated from systems of ODE's.

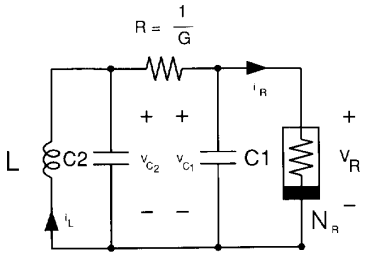

Fig. 3. Chua's circuit.

IV. Experimental Analysis of the Complex Dynamics in Chua's Circuit by Means of 1-D Maps

One of the goals of an experimental study of the nonlinear dynamics of self-excited oscillators is to find bifurcations which can explain the intrinsic oscillation properties of the system. In order to understand the complicated bifurcation scenarios occurring in some dynamical systems with chaotic behavior we need to carry out the analysis of the bifurcations in at least a 2-D parameter subspace. In this case, one can point out the bifurcations of codimension 2,[4] which can give rise to the complicated structure of bifurcations of codimension 1. It is essential that the topological properties of the structures in the neighborhood of the codimension 2 bifurcations are well studied in the theory of bifurcations. The results of this theory can then be effectively applied to experimental studies.

As the experimental tools for the study of autonomous systems with chaotic behavior is well developed (see, for example, [4], [5]), we can use a physical circuit such as Chua's circuit which possesses a rich repertoire of chaotic dynamics to demonstrate some significant results of modern bifurcation theory. It has been shown in numerical simulations [6], [7] and in experimental study [5] that due to the strong dissipative compression of the phase space the return map for the trajectories of some attractors in Chua's circuit can be approximated by means of a 1-D map. In the sequel, the first return map we refer to will not be the 2-D Poincaré map, but the 1-D map that is constructed from the 2-D map by means of a projection. In the figures of experimental results, the return map will be shown by plotting the trajectory using

[4] A bifurcation of codimension 2 refers to the fact that the set of bifurcation points form a manifold in the parameter space with codimension 2, where codimension is the dimension of the parameter space minus the dimension of the manifold.

the coordinates $(x_i, f(x_i))$, where f is the return map and x_i are the successive points of the trajectory on the 1-D map.

The experimental tools used in this paper include the visualization of 2-D projections of the attractors, the plotting of the Poincaré cross-sections and their corresponding 1-D return maps, visualization of the bifurcation diagram, and the periodical switching of the circuit to the (unstable) fixed point for studies of the homoclinic and heteroclinic orbits.

For the experimental demonstrations of the bifurcation phenomena produced by Chua's circuit it is convenient to use the parameters C_1 and R as control parameters (see diagram of Chua's circuit in Fig. 3). Because in previous studies the parameters R and C_1 were not used as control parameters of the system let us briefly consider the simplest bifurcations in the parameter plane (R, C_1). As the inductor has some finite series resistance, we will consider Chua's oscillator [8], [9], which is Chua's circuit with a linear resistor added in series with the inductor. In our case, the resistance of this resistor is small and positive.

The state equations of Chua's oscillator are [10]

$$\begin{cases} C_1 \frac{dv_{C_1}}{dt} = G(v_{C_2} - v_{C_1}) - g(v_{C_1}) \\ C_2 \frac{dv_{C_2}}{dt} = G(v_{C_1} - v_{C_2}) + i_L \\ L \frac{i_L}{dt} = -v_{C_2} - R_0 i_L \end{cases} \tag{2}$$

where G=1/R and the nonlinear function $g(v_{C_1})$, which defines the v–i characteristic of the nonlinear resistor N_R (called Chua's diode [11]), is described by the piecewise-linear function

$$g(v_{C_1}) = G_b v_{C_1} + \tfrac{1}{2}(G_a - G_b)[|v_{C_1} + B_p| - |v_{C_1} - B_p|].$$

The parameters of the function g in the experimental setup, which we keep fixed, are

$$G_a = -0.756 \text{ mS}, \quad G_b = -0.409 \text{ mS}, \quad B_p = 1.05 \text{ V}.$$

The parameter values of the linear elements of Chua's oscillator which we keep fixed are $L = 37.56$ mH, $C_2 = 215$ nF and the measured resistance of the inductor L is equal to $R_0 = 30\ \Omega$.

4.1. Bifurcations of Equilibrium States in the Parameter Plane (R, C_1)

The coordinates of the equilibrium states in the phase space of the system (1) are given by the solutions of the equations:

$$\begin{cases} G(v_{C_2} - v_{C_1}) - g(v_{C_1}) = 0 \\ G(v_{C_1} - v_{C_2}) + i_L = 0 \\ v_{C_2} + R_0 i_L = 0. \end{cases} \tag{3}$$

The origin is always an equilibrium state. The number of equilibrium states is equal to the number of solutions of

$$G\left(\frac{R_0}{R_0 + R} - 1\right) v_{C_1} - g(v_{C_1}) = 0. \tag{4}$$

For example, in the case of when $R_0 = 0$, $G_a < G_b < 0$, $G > 0$ (such as the case considered in [6]), if $R < -1/G_a$ or $R > -1/G_b$ then the system (1) has only one equilibrium state $O_0(0, 0, 0)$. When $-1/G_a < R < -1/G_b$ there are two additional equilibrium states $O_+(v^0_{C_1}, v^0_{C_2}, i^0_L)$ and $O_-(-v^0_{C_1}, -v^0_{C_2}, -i^0_L)$ in the phase space of the system.

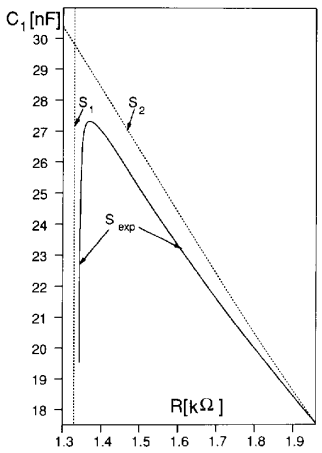

Fig. 4. Stability borders of the equilibrium points $0_-, 0_+$ in (R, C_1) parameter plane.

In the general case, the coordinates of the points O_+ and O_- are given by the expression:

$$\begin{cases} v^0_{C_1} = \frac{(G_b - G_a)RB_p}{1 + RG_b - \frac{R_0}{R+R_0}} \approx \frac{(G_b - G_a)RB_p}{1 + RG_b} \\ v^0_{C_2} = \frac{R_0}{R+R_0} v^0_{C_1} \approx 0 \\ i^0_L = \frac{-1}{R+R_0} v^0_{C_1} \approx \frac{-1}{R} v^0_{C_1} \end{cases} \tag{5}$$

where the approximations are given for the case when R_0 is small relative to R. In the sequel, we will only consider the parameter region restricted by the condition $R < -1/G_b$.

The eigenvalues of the linear system in the regions of the points O_+ and O_-, which we shall call the outer regions, are given by the characteristic equation:

$$\begin{aligned} &LC_1C_2p^3 + (C_1C_2R_0 + LC_1G + LC_2G + LC_2G_b)p^2 \\ &\quad + [(C_1G + C_2G + C_2G_b)R_0 + LGG_b + C_1]p \\ &\quad + R_0G_bG + G + G_b = 0. \end{aligned}$$

Using the Routh method, one can find that the equilibrium states O_+ and O_- are stable if the parameter values of the system (2) satisfy the following condition:

$$\begin{aligned} &[C_1(C_2R_0 + LG) + LC_2(G + G_b)] \\ &\quad \cdot [(C_1G + C_2G + C_2G_b)R_0 + LGG_b + C_1] \\ &\quad > LC_1C_2(R_0G_bG + G + G_b) \end{aligned} \tag{6}$$

On the parameter plane this border of stability is shown by the curve S_2 (see Fig. 4). The line S_1 on the plane corresponds to the border where the equilibrium states O_+ and O_- disappear:

$$\left(G\left(1 - \frac{R_0}{R_0 + R}\right) = -G_a\right).$$

In any physical implementation, Chua's oscillator has a Chua's diode whose v-i characteristic is smooth. If we assume that there are at most three equilibrium points, then the equilibrium points O_+ and O_- do not disappear suddenly

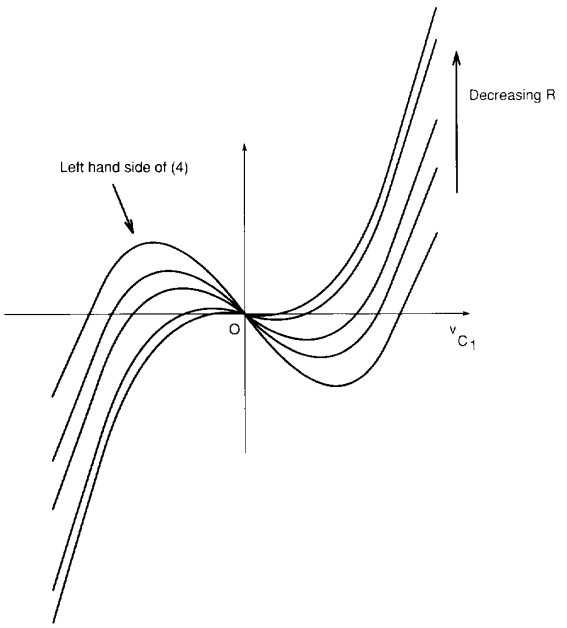

Fig. 5. Left-hand side of (4) for different values of R.

but approach and merge into the origin. This is shown in Fig. 5, which plots the left hand side of (4) for different parameter values. Therefore, the stability border S_{exp} consists of a single curve instead of the two lines S_1, S_2. Furthermore, due to other parasitic components which we did not take into account, the stability border S_{exp} found in the experiment deviates slightly from S_1 and S_2. The curve S_{exp} corresponds to the loss of stability of O_+ and O_- through an Andronov–Hopf bifurcation.[5] In the model (2) S_2 corresponds to an Andronov–Hopf-like bifurcation as well and S_1 indicates the birth of an unstable equilibrium point and a stable limit cycle due to boundary effects of the piecewise-linear function $g(x)$.

Due to the odd-symmetry of the nonlinearity of Chua's diode N_R the model of Chua's circuit is invariant with the state variable transformation T_S: $(v_{C_1}, v_{C_2}, i_L) \rightarrow (-v_{C_1}, -v_{C_2}, -i_L)$. As a result of this symmetry every nonsymmetric (with respect to the origin) limit set in the phase space of the circuit coexists with a similar limit set obtained from the first one by means of the transformation T_S. In order to distinguish between these nonsymmetric limit sets we will use the subscript "−" and "+". For example O_-, O_+ will denote the two equilibrium points, P_+ and P_- denote two limit cycles and CA_+ and CA_- denote any two chaotic attractors which are symmetric with respect to each other. With the exception of O_0, the symbols for the symmetric limit sets will not contain such subscripts.

[5] An Andronov–Hopf bifurcation says that an equilibrium point gives birth to a periodic solution when a pair of complex eigenvalues of the linearized system crosses the imaginary axis nontangentially as some parameter is varied. In the literature, the Andronov–Hopf bifurcation is proved for sufficiently smooth systems.

We will now show the results of our experimental study of bifurcation phenomena occurring in Chua's circuit.

4.2. Experimental Setup

In our experiments we synthesize the Chua's diode N_R using the approach described in [11].

The setup for generating the Poincaré cross section and the 1-D map is shown in Fig. 6(a). The Poincaré cross section circuit finds when the state crosses the Poincaré plane and records a projection of the state. In our case, the projection is just $v_{C_1}(t)$. This projection is then used by the 1-D map circuit to generate the 1-D map, by recording the projections of subsequent crossings of the trajectory through the Poincaré plane.

The setup for generating the bifurcation diagrams is shown in Fig. 6(b). A sawtooth waveform is used to control a voltage-controlled capacitor in order to periodically sweep the parameter space. This waveform is also used for tracking control in the oscilloscope. For more details on these circuits, the reader is referred to the Appendix.

The setup for generating pictures of homoclinic and heteroclinic orbits is shown in Fig. 6(c). A periodic pulse is used to periodically set the initial state near the origin by short-circuiting the active Chua's diode N_R (making the origin in the resulting system asymptotically stable) via a relay.

In Fig. 7, we show how the 1-D map is generated experimentally. In Fig. 7(a), $U_\Sigma = U_o$ denotes the Poincaré plane which is parallel to the i_3 axis. The numbers 1 to 3 shows three trajectories originating from the points y^1 to y^3 on the Poincaré plane respectively. These trajectories intersect the Poincaré plane again at the points z^1 to z^3. The projection of these points on the v_{C_1} axis (i.e., y^1 is projected to x^1, etc.) will be used in the 1-D map, whose graph is shown in Fig. 7(b).

We note in Fig. 7(a) that the projection is not one-to-one. Two points in the Poincaré cross section are projected onto the same point. Thus the Poincaré cross section is not completely flat. This is what is meant by the 1-D map being only an *approximation* for the 2-D map. We also note that the 1-D map in Fig. 7(b) is not invertible, because it is not one-to-one. For 1-D maps, not being one-to-one is an important ingredient for generating chaotic and bifurcation behaviors, as it generally implies stretching of the phase space by the map. This is especially true for continuous 1-D maps, as injective continuous 1-D maps are necessarily monotone and thus does not have much interesting dynamics. As Chua's circuit has a piecewise-linear vector field, we have global uniqueness and existence of trajectories. Therefore, the Poincaré map as defined is one-to-one. Thus in order for the 1-D map obtained not to be one-to-one, the projection should not be one-to-one as well. This give some justification why the projection "should" not be one-to-one.

4.3. Period-Doubling Route to Chaos

In Fig. 8, we show our results of the experimental study in the two-parameter plane (R, C_1). It has been shown in a number of papers (see, for example, [6]) that a period-doubling

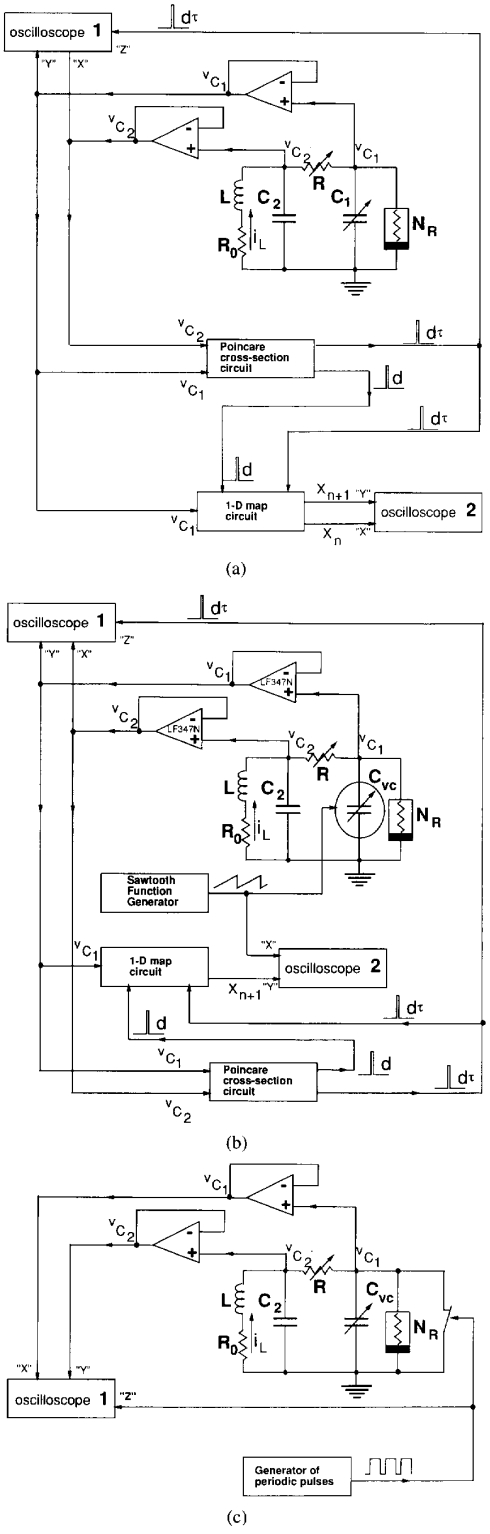

Fig. 6. Schematic diagram of experimental setup: (a) Setup for analyzing Poincaré cross section on oscilloscope 1 and 1-D map on oscilloscope 2 of the attractors; (b) setup for generating bifurcation diagrams on oscilloscope 2. Oscilloscpe 1 is used to control the Poincaré cross sections; (c) setup for generating pictures of homoclinic and heteroclinic orbits.

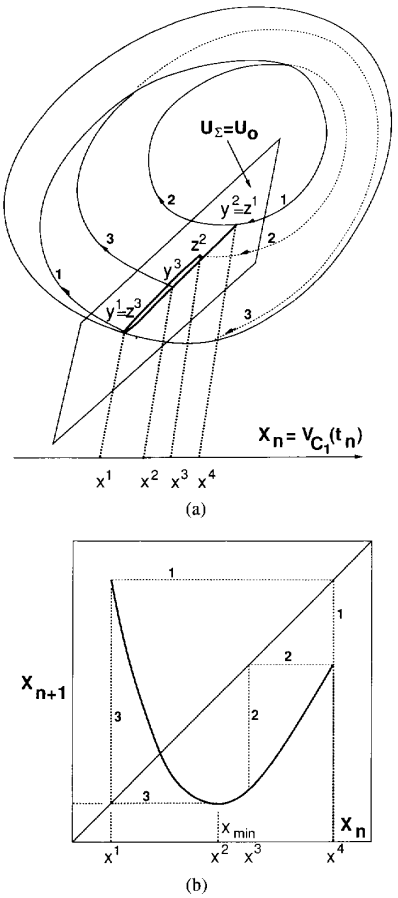

Fig. 7. Construction of 1-D map through a projection of the Poincaré cross section in the experimental study: (a) Projection of attractor from 2-D Poincaré cross section onto 1-D line; (b) graph of 1-D map.

sequence from a pair of periodic orbits P_+ and P_- precede the appearance of chaos in Chua's circuit.

In our experimental study on the parameter plane (R, C_1), this bifurcation scenario is observed if we vary the parameters along a curve which intersects the curves h_1, h_2, and h_{cr}.[6] In this case, the stable limit cycles P_+ and P_-, appearing through an Andronov–Hopf bifurcation from the equilibrium states O_+ and O_-, undergoes a period-doubling bifurcation at the curve h_1, where these limit cycles lose stability and new stable periodic orbits $2P_+$ and $2P_-$ appear that has approximately a period twice as long. In order to distinguish between the different periodic orbits generated by Chua's circuit, we use a numerical index before the symbols P_+ or P_-. This index shows the number of revolutions before the periodic orbit returns to its starting point. This corresponds to the number of intersection points with an appropriate Poincaré cross section. For an appropriately chosen Poincaré map there is then a correspondence between a periodic limit

[6]The symbol h is used to denote the border where a period-doubling bifurcation occurs. The symbol h_n denotes bifurcation points at which the stable period-n limit cycles loses stability when one characteristic multiplier crosses the value -1.

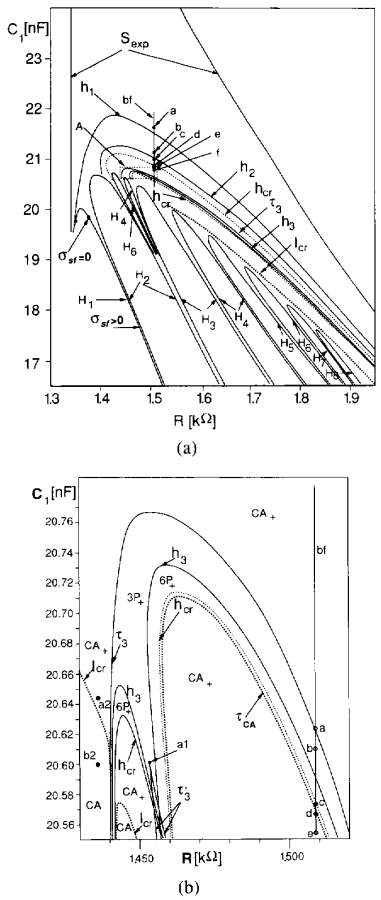

Fig. 8. (a) Experimental bifurcation curves of Chua's oscillator in (R, C_1) plane; (b) enlargement of area A in Fig. 8(a).

cycle nP_+ of the continuous-time flow and a periodic point of period n of the Poincaré map. Since the limit cycle moves when we vary parameters, in the experiment we adjust the Poincaré cross section to follow this motion in order to get an appropriate Poincaré cross section. The projections of the limit cycles P_+ (before the bifurcation) and $2P_+$ (after the bifurcation) onto a 2-D display and the corresponding first-return maps of these periodic orbits are shown in Fig. 9(a)(b). The parameters values denoted by a through f on the line bf in Fig. 8(a) correspond to the attractors shown in Fig. 9(a)–(f), respectively.

The next period-doubling bifurcation takes place when we vary the parameters of the circuit across the curve h_2. As a result of this bifurcation the limit cycles $2P_+$ and $2P_-$ lose their stability and new stable periodic orbits $4P_+$ and $4P_-$ appear (Fig. 9(c)).

Due to the influence of physical and measurement noise only three or four consecutive bifurcations can usually be observed in experiments before chaos emerges on the curve $h_{\rm cr}$, although theoretically, an infinite number of bifurcation occurs between h_2 and $h_{\rm cr}$. Note that the trajectory of the chaotic attractors appearing immediately after this transition to chaos produces a return map which has almost a 1-D structure (Fig. 9(d)(e)(f)).

Varying the parameters further towards more developed chaos shows that the experimentally obtained return map can be well approximated by a 1-D map which is very close to the logistic map. This means that the behavior of the trajectories on the attractors and the bifurcations of the attractors with respect to parameter variations in the vicinity of the curve $h_{\rm cr}$ are in accordance with the Feignbaum scenario.

Fig. 10 shows an experimentally obtained bifurcation diagram with the parameter C_1 decreasing along the line bf in Fig. 8. From this bifurcation diagram we see that the sequence of bifurcations is very similar to the bifurcations occurring in the logistic map (Fig. 1).

After the appearance of chaos further parameter variation reveals a sequence of chaotic and stable periodic regions. In the experimental bifurcation diagram one can see a region of stable period-3 limit cycles located between chaotic regions. The narrow regions of the parameters corresponding to stable periodic limit cycles surrounded by regions of chaos are called *periodic windows*.

4.4 Intermittency and Periodic Windows

Let us consider the bifurcations bordering the period-3 window. The results of the experimental study of the period-3 windows in the two-parameter plane (R, C_1) are presented in Fig. 8(b). This figure is the enlargement of area A from Fig. 8(a). The attractor projections and corresponding return maps for the parameter values taken along the line bf, which crosses the period-3 window, are shown in Fig. 11. These attractors are presented in the order of decreasing C_1. The points a through e on the line bf in Fig. 8(b) are parameter values which corresponds to the attractors shown in Fig. 11(a)–(e), respectively.

Immediately before the appearance of a stable limit cycle $3P_+$, an intermittent phenomenon is observed, as is shown in Fig. 11(a). This phenomenon is a form of chaos. This form of chaos is called intermittency because except for an irregular appearance of short intervals of spurious bursts, the time waveforms are virtually periodic. This can be seen in Fig. 12, where the discrete time trajectory of the attractor taken from the 1-D map is shown. This route to chaos, where intermittency appears after the bifurcation, is referred to as the *intermittency route to chaos*.

The curve τ_3 denotes the bifurcation parameters associated with the appearance of a period-3 limit cycle.[7] The phase portrait of the stable limit cycle $3P_+^s$ is shown in Fig. 11(b).

The analysis of 1-D maps obtained from limit cycles and intermittent chaotic attractors enables us to conclude that on the curve τ_3 the limit cycle $3P_+^s$ loses stability because one of its characteristic multiplier crosses the value $+1$. This conclusion follows from the fact that at the critical parameter value, two points (an even number) of this cycle lie on the decreasing part of the return function; see Fig. 11. As a result,

[7]The symbol τ is used to denote bifurcation points where a tangent bifurcation takes place.

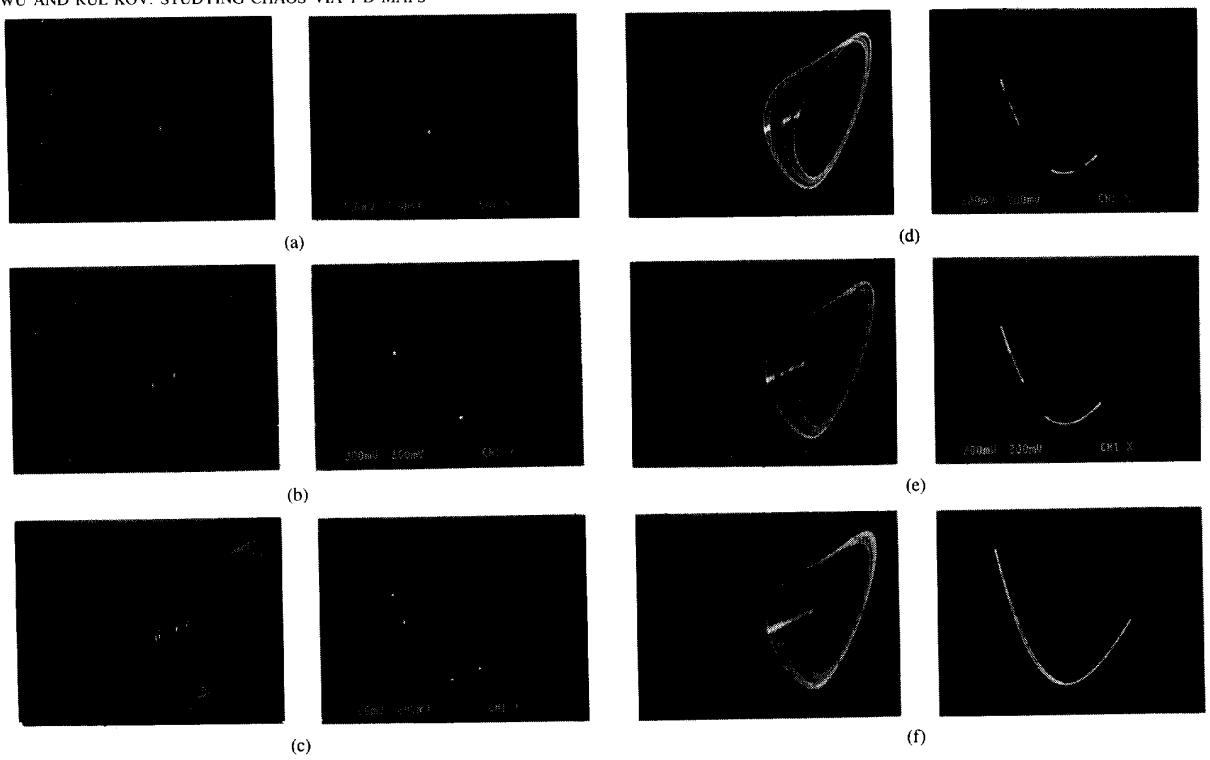

Fig. 9. Attractors in period-doubling route to choas. The Poincaré cross section is shown by bright points on the oscilloscope screen along with the trajectory (left picture). The corresponding 1-D map is shown in the right picture.

we can say that the above intermittent behavior corresponds to an intermittency of type 1 [12].

When the parameters of the system approach the curve τ_3 (see Fig. 8(b)) the appearance of irregular bursts in the waveform becomes less frequent. It follows from the theory of intermittency (see, for example, [12]), that for the type of intermittency considered above, the average time between bursts grows proportionally to $(\alpha - \alpha_{\rm cr})^{-1/2}$, where $\alpha_{\rm cr}$ is the critical parameter value when the oscillations cease to be periodic. In our case the values of the control parameters R or C_1 can be considered as the parameter α, and the parameter values taken on the curve τ_3 as $\alpha_{\rm cr}$.

On the border τ_3 the stable limit cycle $3P_+^s$ merges with an unstable limit cycle $3P_+^u$ and disappears. This means that a tangent bifurcation has taken place on the curve τ_3 and at least four periodic limit cycles $3P_+^s$, $3P_-^s$, $3P_+^u$, and $3P_-^u$ coexist in the phase space of Chua's circuit when the parameter values are chosen inside the period-3 window. The occurrence of a tangent bifurcation is shown in Fig. 13(a), where a map is shown for three different parameter values. The stable and unstable fixed points are denoted by s and u respectively. As the parameter is varied, the stable and unstable fixed points merge and disappear as the characteristic multipliers approach 1. In Fig. 13(b) we show the third iterate ($f^{(3)}$) of a computer-generated 1-D map from Chua's oscillator right after $3P_+^s$ has merged with $3P_+^u$ and disappeared. As can be seen from the figure, a tangent bifurcation has indeed taken place. This mechanism also occurs in the period-3 window of the logistic map.

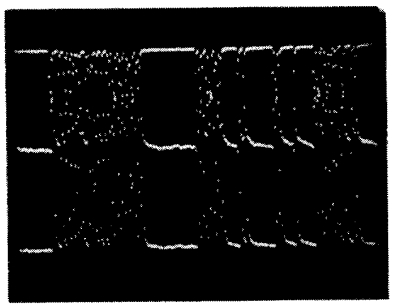

Fig. 10. Experimentally obtained bifurcation diagram. The horizontal axis is the parameter C_1 =21.6 nF down to C_1 =20.4 nF. The vertical axis is v_{c_1}. The resistance of R is 1543 Ω.

Detailed analysis of the 1-D map shows that when the parameter values changes from the border τ_3 down to the border h_3, the lowest point of the limit cycle moves through the minimum of the 1-D map and enters the interval where this map has a positive slope. After that only one point (odd number) of the limit cycle is located on the decreasing part of the map. This means that the characteristic multiplier of the limit cycle becomes negative. When the limit cycle loses its stability on the border h_3, the characteristic multiplier stays negative and goes through the value -1. As a result of this the period-doubting bifurcation gives birth to a stable limit cycle $6P_+$. Then a sequence of period-doubting bifurcations leads to the appearance of the 3-band chaotic attractor CA_+ shown in Fig. 11(c).

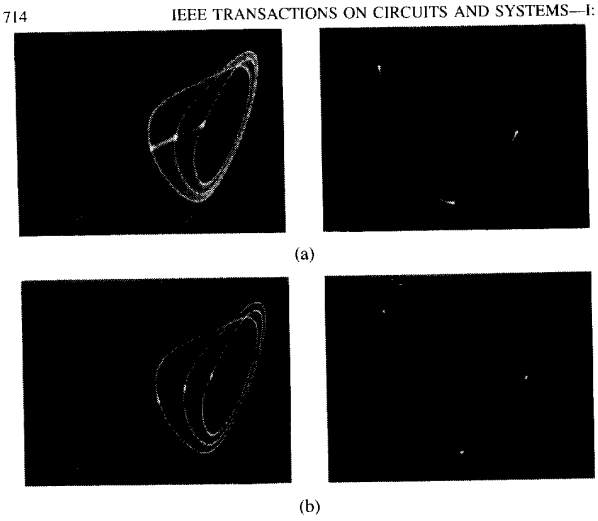

Fig. 11. Phase portraits of attractors generated by Chua's oscillator in the vicinity of period-3 window: (a) and (b).

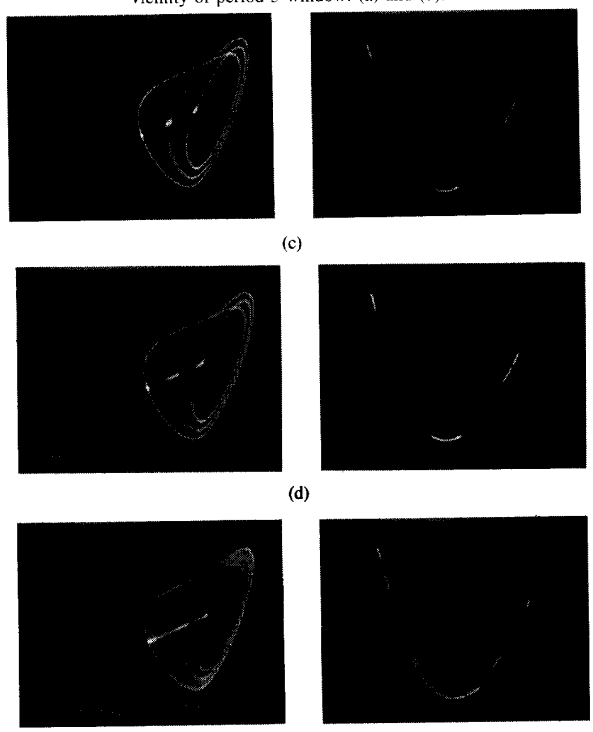

Fig. 11. (Continued): (c)–(e).

Further evolution of chaos by parameter variation results in a crisis phenomenon which leads to the sudden extension of the three-band chaotic attractor CA_+ (Fig. 11(c) and (d)), in the sense that the trajectory which was confined to 3 disjoint regions suddenly occupies a large area of phase space. This phenomenon is explained by the collision of the 3-band chaotic attractor CA_+ with the unstable limit cycle $3P_+^u$. This collision is the result of complicated phenomena caused by interactions between the stable and the unstable manifolds of the limit cycle $3P_+^u$ [13]. In the intermittency scenario considered earlier, the trajectory becomes intermittently periodic and chaotic (Fig. 12). In the case here, after the collision, the trajectory is intermittent in the region where the 3-band chaotic attractor used to be, and in a much larger region of phase space, moving chaotically in each region. This is called *chaos–chaos type intermittency*. In Fig. 14(a), we show the discrete-time trajectory of the 1-D map of the 3-band chaotic attractor CA_+ before the collision. In Fig. 14(b), we observe intermittency after the collision, where the trajectory stays in the 3-band region most of the time, but sometimes leaves this region. In Fig. 14(c), the parameter is further varied and the attractor fills up a larger region of the phase space. Again, this phenomena occurs in the period-3 window of the logistic map as well.

We have considered the bifurcations on the borders of the period-3 window obtained by varying the parameter C_1 along the line bf. In the parameter range considered, the function of the 1-D map model has a simple shape with a single extremum (Fig. 11(e)). This function can be approximated by a quadratic function and, as a result, the dynamics of the system in the

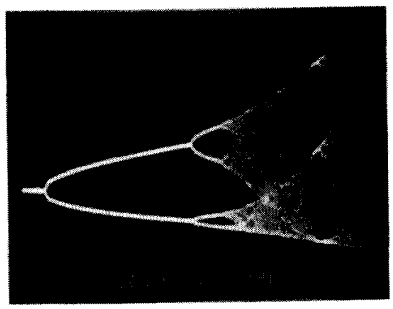

Fig. 12. One-dimensional map iterates versus time corresponding to Fig. 11(a). We see long periods of period-3 behavior interrupted by irregular chaotic bursts.

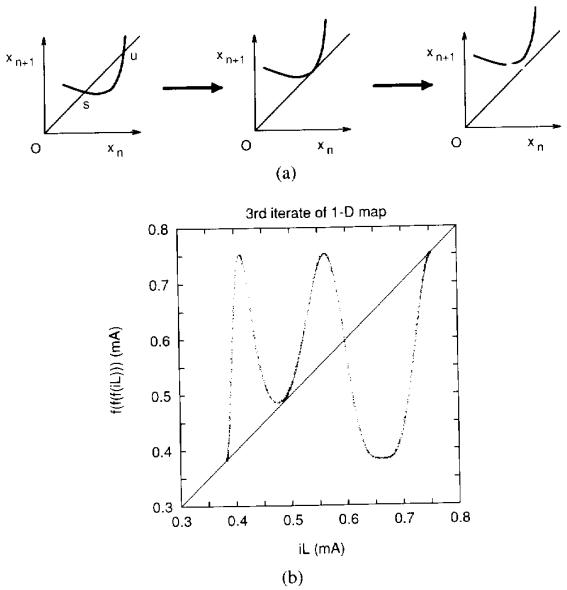

Fig. 13. (a) Occurence of tangent bifurcation. The stable fixed point s and the unstable fixed point u merges and disappears as a parameter is varied; (b) computer-generated third iterate of 1-D map from Chua's oscillator after period-3 points have disappeared.

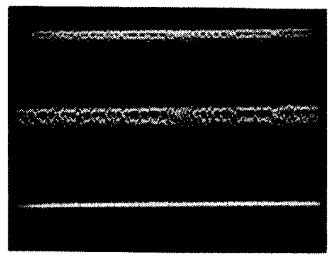

(a)

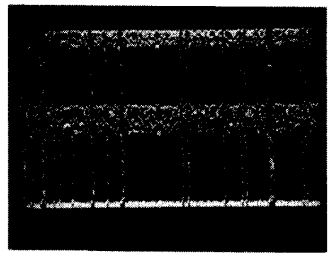

(b)

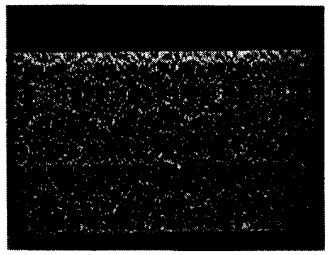

(c)

Fig. 14. One-dimensional map iterates versus time of attractors shown in Fig. 11(c)–(e): (a) Three-band attractor CA_+ before collision with unstable periodic limit cycle (Fig. 11(c)); (b) intermittency occuring after collision (Fig. 11(d)); (c) 1-D map iterates fill up large area of phase space (Fig. 11(e)). Trajectory is not confined to the a-band region.

vicinity of the window can be understood with a one-parameter study. However, when we consider the dynamics in a larger region of the parameter space, we find that the function of the 1-D map becomes more complicated. In particular, new extrema of the function appears which plays a role in the behavior of the attractors (see Fig. 15(a)). Due to this fact, a two-parameter study is required in order to understand the bifurcation scenario.

Consider Fig. 8(b). We can see that the region of stability of $3P_+$ and $3P_-$ has four long and narrow branches. Two of these branches overlap starting from the point $a1$. The point $a1$ corresponds to a bifurcation of codimension 2. This bifurcation gives rise to a tangent bifurcation of codimension 1, which are indicated by the curves τ_3'. These tangent bifurcations lead to the appearance of pairs of additional limit cycles of period 3: $3P_+^s$, $3P_-^s$, $3P_+^u$, and $3P_-^u$. Hence the region of the parameters located in the polygon between τ_3' and h_3 corresponds to the case where there are at least eight period-3 limit cycles coexisting in the phase space of the system.

The experimental results presented here demonstrate common features of periodic windows in dynamical systems

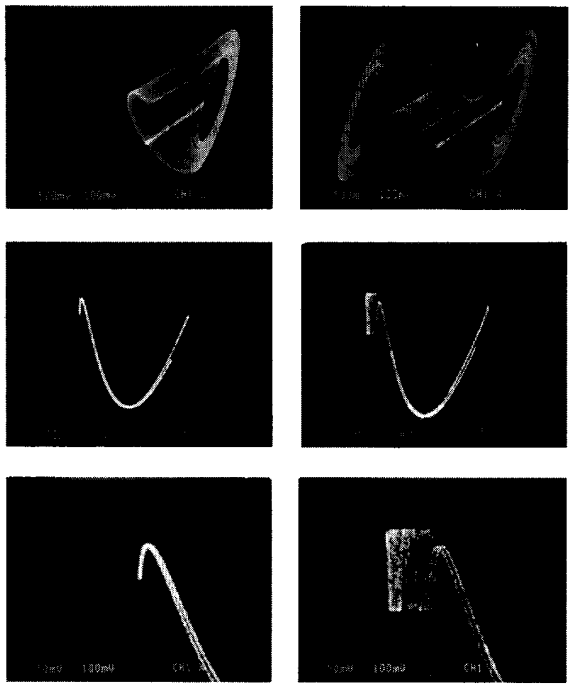

(a) (b)

Fig. 15. Phase portraits, the corresponding 1-D maps, and detailed views of the 1-D maps near discontinuity for CA_+ and CA. The parameter values are denoted in Fig. 8(b): (a) Point a2 in Fig. 8(b); (b) point b2 in Fig. 8(b).

described by 1-D maps with more than one extrema. The theoretical background of these results can be found in [14], [15].

4.5. 1-D Maps of the Double Scroll Chua's Attractor

To further explore the intrinsic properties of 1-D maps generated by Chua's circuit let us consider the evolutions of the attractors and the corresponding 1-D maps when the parameter C_1 is in the region of the double scroll Chua's attractor. The results of this experiment are presented in Fig. 15.

The main difference between the 1-D maps generated by the chaotic attractor CA_+ and the double scroll Chua's attractor CA is that the 1-D maps of CA has a discontinuity which splits the return-map function into two parts. The discontinuity of the 1-D map results from the behavior of the trajectories in the neighborhood of the saddle-focus O_0 which is located at the origin of the phase space. Let a be the point where the 1-D return map has a discontinuity. The trajectories originating from the Poincaré section of the double-scroll Chua's attractor CA are separated by the 2-D stable manifold of the saddle-focus O_0 into two parts: part A where $X > a$ and part B where $X < a$ (Fig. 16). The point a itself lies on the stable manifold of the origin and its trajectory will not intersect the Poincaré plane again. Starting from a point on the Poincaré plane corresponding to part A, the behavior of the trajectories until the next intersection point in part A of CA is similar

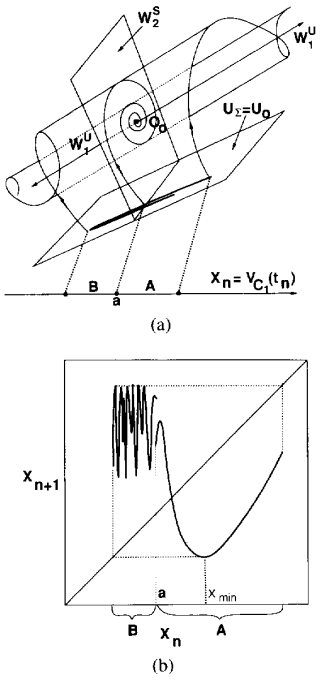

Fig. 16. Construction of 1-D map in double-scroll Chua's attractor region: (a) 2-D stable manifold of $O_0(W_2^s)$ separates the trajectories of the attractor into two parts with qualitatively different behavior. 1-D unstable manifold of O_0 is denoted W_1^u; (b) graph of constructed 1–D map.

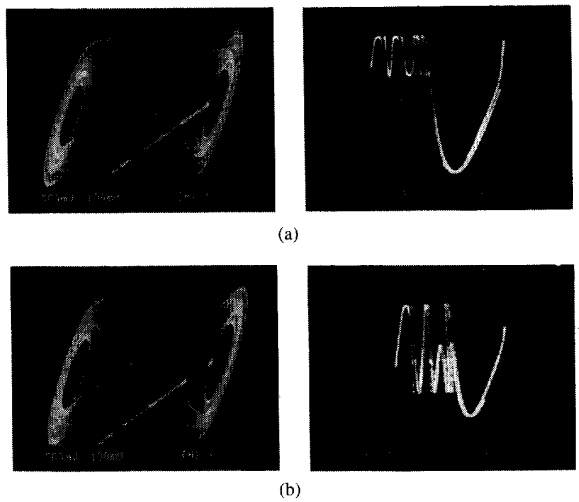

Fig. 17. Examples of the double-scroll Chua's attractor and the corresponding 1-D maps measured from experiments: (a) C_1= 16 nF, r= 1.59 kΩ; (b) C_1= 16 nF, r= 1.54 kΩ.

to the trajectories of CA_+. However, the trajectories starting from part B can have a rather complicated behavior in the left part of the phase space, before they intersect the Poincaré plane again. This behavior give rise to the complicated oscillatory structure of the 1-D map in the domain $X < a$ (see Figs. 16(b) and 17(a), (b)). The complex shape in part B is very sensitive to parameter changes in comparison with the shape of part A.

As mentioned before, we obtained a 1-D map from the 2-D Poincaré map through a projection. For the projection we chose, the trajectories of the attractors which go from the Poincaré cross-section to the stationary state O_0 map approximately into the single point a. This enable us to consider the point a in the 1-D map model as the image of the 2-D stable manifold of the saddle-focus O_0. Due to physical noise in the experimental set-up, the trajectories on the manifold can not stay on the stable manifold of the saddle-focus O_0 and they will move along the 1-D unstable manifold of O_0 either to right or to left. If the trajectory goes to the right, then the next intersection with the Poincaré section will give us the point $f(a)$, which is the image of the 1-D unstable manifold W_1^u intersecting the Poincaré plane. As we know which trajectories of the 1-D map correspond to the manifolds of O_0, we can study the bifurcations connected with the manifolds directly from the 1-D map. Such bifurcations give rise to homoclinic orbits[8] associated with the saddle-focus O_0.

In the 3-D phase space of Chua's circuit these homoclinic orbits are the trajectories which converge to O_0 along W_1^u as $t \to -\infty$, and which converge to O_0 along W_2^s as $t \to \infty$. From the point of view of the 1-D map model, the homoclinic orbit is the closed orbit which contains the point a. For example the image of the homoclinic orbit H_n[9] in the 1-D map is the trajectory which satisfy the following conditions: $a = f^{(n)}(a)$, $f^{(j)}(a) > a$ where $j = 1, \cdots, (n-1)$. Examples of 1-D maps which satisfy these conditions are shown in Fig. 18(a), (b) for the cases $n = 1$ and $n = 2$, respectively.

Another bifurcation connected with the manifolds of O_0 is the crisis phenomenon [16]. As the result of the crisis, the twin chaotic attractors CA_+ and CA_- merge together (CA_+ is shown in Fig. 15(a)), thereby giving birth to the odd-symmetric attractor CA shown in Fig. 15(b). In the R, C_1 parameter plane the bifurcation curve of the crisis is denoted by l_{cr}, see Fig. 8(a), (b). When the parameters of the circuit lies on the bifurcation curve l_{cr}, the trajectory belonging to the attractor CA_+ and originating from the minimum point on the 1-D map, is mapped into the point a, i.e., $a = f(X_m)$, where $X_m = \min_{X \in CA_+}\{f(X)\}$.

A detailed analysis of the 1-D map and the topological properties of the trajectories in the phase space enables one to make the following conclusions. Before the crisis, $a < X_{\min} = \min_{X>a}\{f(X)\}$, thus if $X \in A$, then the trajectory of X via the 1-D map f remains in A. This means that the 2-D stable manifold W_2^s of O_0 separates the basins of attractions of CA_+ and CA_-. In this case, any trajectory from one side of the stable manifold can never go to the other side. Observe that in the 1-D map model the entire stable manifold W_2^s is mapped into point a. After the crisis, the trajectories of the symmetric attractor CA can go from one side of W_2^s to the

[8] A homoclinic (heteroclinic) orbit is the orbit, both forward and backward, of a point whose forward time and backward time trajectory both converge to the same equilibrium point (different equilibrium points). In other words, a homoclinic (heteroclinic) orbit lies on the intersection of stable and unstable manifolds of equilibrium points. Typically, when we talk about homoclinic or heteroclinic orbits the associated equilibrium points are saddle points.

[9] On the parameter plane, the symbol H_n denotes the parameter set where the system contains the corresponding homoclinic orbit.

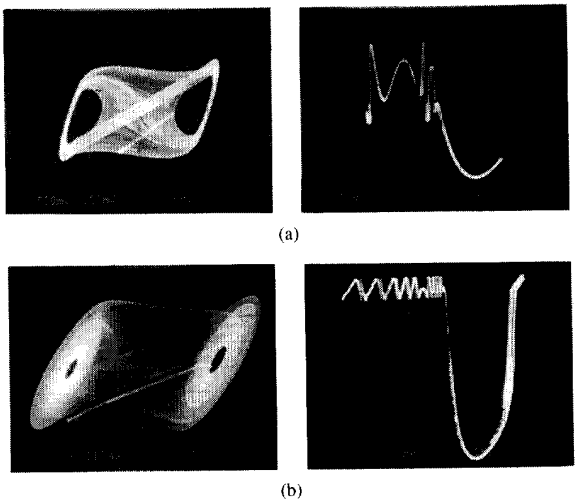

Fig. 18. Attractors and 1-D maps generated by the bifurcation parameters at homoclinicity located on the curves H_n: (a) H_1: The parameter values are shown by arrow from H_1 (Fig. 8(a)); (b) H_2: The parameter values are shown by right arrow from H_2 (Fig. 8(a)).

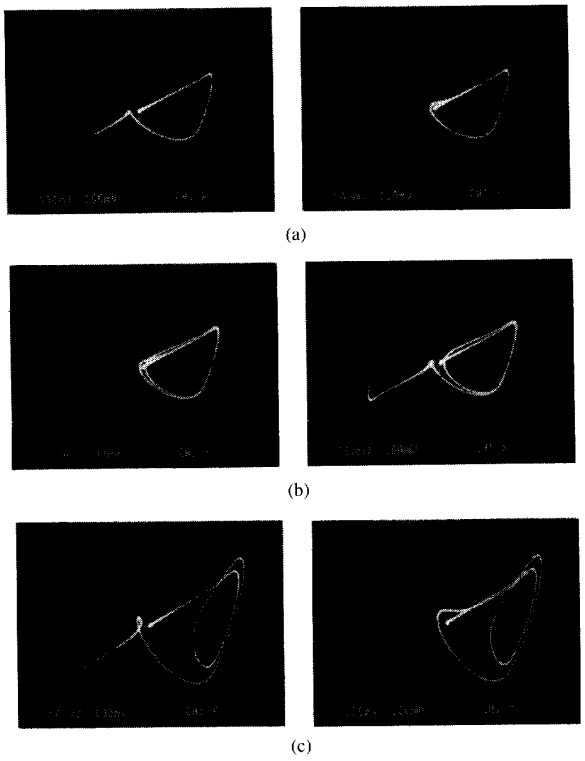

Fig. 19. Behavior of the trajectories located in the 1-D unstable manifold of the saddle focus O_0: (a) Parameter of the circuit is taken from the left and right of the value on bifurcation curve H_1 pointed by arrow from H_1 in Fig. 8(a); (b) parameter of the circuit is taken from the left and right of the left arrow of H_2 in Fig. 8(a); (c) parameter of the circuit is taken from the left and right of the right arrow of H_2 in Fig. 8(a)

other. This implies that at least one homoclinic bifurcation associated with the saddle-focus O_0 must occur before the crisis phenomenon where CA_+ and CA_- collide. After the crisis, $a > X_{\min} = \min_{X>a}\{f(X)\}$. Thus there is a region in A that will get mapped into B. The size of this region increases as the parameter is further away from the crisis point. When this region is small, it means that the trajectory will stay in A for a time and occasionally switch to B and vice versa. In the 3-D flow, this appears as trajectories which looks like CA_+ switching to trajectories which looks like CA_- and vice versa. This is also a form of chaos–chaos intermittency.

The analysis of the 1-D maps obtained from the experimental study enables us to make the following conclusions concerning the structure of the chaotic attractors. Because the return-map function has many local extremum points (see Figs. 15, 17, 18), many stable limit cycles can exist in the parameter region corresponding to CA_+ and CA. Stable limit cycle associated with multiple local extrema of a 1-D map can have long periods and extremely complicated yet very narrow basins of attraction. These features make them almost unobservable in experiments and numerical simulations. Despite their local stability any small noise will throw a periodic trajectory out of its basin, and as a result, this trajectory will land in a domain of complicated transient behavior. In this case the oscillations of the circuit can remain chaotic with the simultaneous coexistence of stable limit cycles in the attractor. These kinds of chaotic attractors are called *quasiattractors* [17].

4.6. Homoclinic and Heteroclinic Orbits Associated with the Saddle-Focus O_0

As mentioned before, the evolution of the experimentally measured 1-D maps when a control parameter is varied shows that there are bifurcation values where homoclinic orbits originating from O_0 exist.

In order to demonstrate the structure of the bifurcation sets corresponding to homoclinicity we show here results of experiments where Chua's circuit is periodically switched to initial conditions in the neighborhood of O_0. The topologically different behaviors of trajectories emanating from 1-D unstable manifold of O_0 in the 3-D phase space are shown in Figs. 19 and 20 in the cases when the parameters of the oscillator are taken from different sides of the bifurcation curves of homoclinic orbits H_n.[10] These parameter values are indicated by the arrows from H_n in the parameter diagram in Fig. 8(a).

Although we consider only a few homoclinic orbits which are easier to study, the structure of the resulting bifurcation sets enable us to conclude that our results are in accordance with well-known theoretical results [18]. This structure of the bifurcation sets is typical for the case when the bifurcation curve H_1 associated with the principal homoclinic orbit has a point in which the saddle-focus value $\sigma_{sf} = \lambda_1 + \lambda_2$ (where λ_1, $\lambda_2 + i\omega_2$ and $\lambda_2 - i\omega_2$ are the eigenvalues of the equilibrium point O_0) changes sign. In Fig. 8(a) the point $\sigma_{sf} = 0$ on the curve H_1 is estimated from experimental study. It was found that only above this point will the stable limit cycles P_- and P_+ smoothly transform into a pair of homoclinic orbits originating from O_0 and then to the stable

[10]The subscript n refers to the number of loops in the homoclinic orbit.

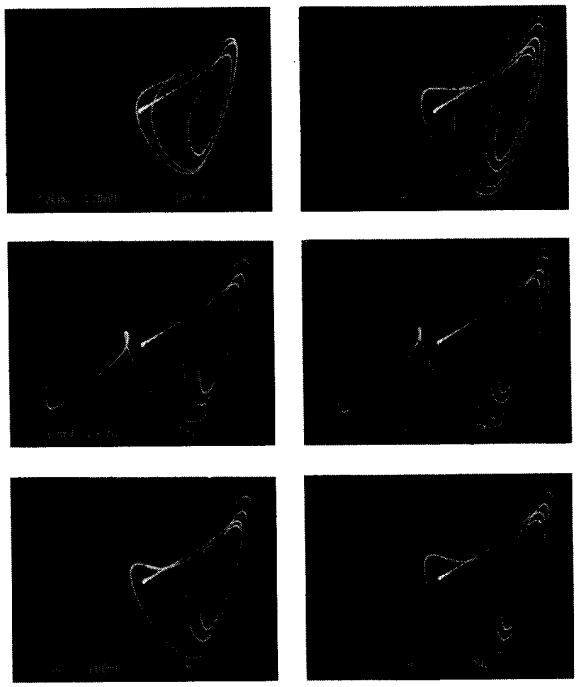

(a) (b)

Fig. 20. Qualitatively different behavior of trajectories in W_1^u of saddle focus: (a) Before and after bifurcations H_3. The parameters are taken to the left of the left arrow from H_3, between the two arrows from H_3, and to the right of the right arrow from H_3, respectively (Fig. 8(a)): (b) before and after bifurcations H_4. The parameters are taken to the left of the left arrow from H_4, between the two arrows from H_4, and to the right of the right arrow from H_4, respectively (Fig. 8(a)).

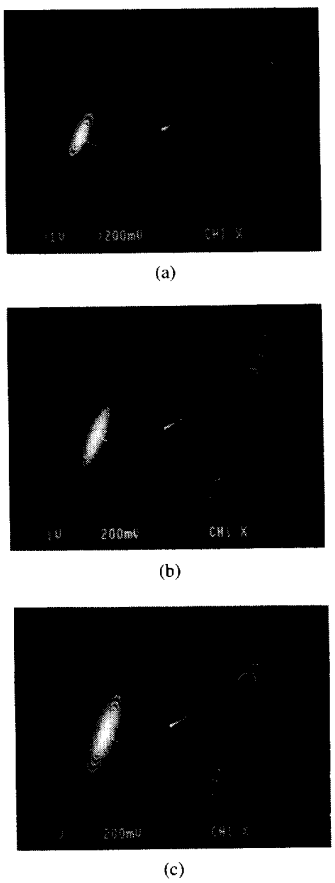

(a) (b) (c)

Fig. 21. Behavior of W_1^u of the saddle focus O_0 when the parameters of the circuit are taken in the vicinity of heteroclinic orbits from O_0 to O_-: (a) C_1= 12.8 nF, R= 1.95 kΩ; (b) C_1= 15.72 nF, R= 1.78 kΩ; (c) C_1= 17.2 nF, R= 1.739 kΩ.

odd symmetric limit cycle P when the parameter values cross the bifurcation curve H_1. As it follows from Shilnikov's theorem [19] a stable limit cycle can be spawned from the homoclinic orbit if $\sigma_{sf} < 0$.

When the parameters of the circuit are taken on the curve H_1 below the point $\sigma_{sf} = 0$, the circuit generates the chaotic attractor CA whose trajectory passes near O_0. This enable us to conclude that there exists a nontrivial hyperbolic set in the neighborhood of the homoclinic orbit H_1. Hence σ_{sf} in this region is positive [19].

The point $\sigma_{sf} = 0$ on the curve H_1 is a bifurcation set of codimension 2. This bifurcation is responsible for the typical structure of the resulting bifurcation sets of codimension 1, which contains the parameter values associated with the homoclinic orbits H_n [18], see Fig. 8(a).

The other examples of the bifurcation sets of codimension 2 found from Chua's circuit are presented in Fig. 21. These figures show the *heteroclinic* trajectory which converges to O_0 as $t \to -\infty$ along W_1^u, and which converges to O_- as $t \to \infty$ along the 1-D stable manifold of O_-. Due to the symmetry of the system, there exist a similar trajectory from O_0 to O_+ as well.

Taking into account the fact that saddle-foci O_0 and O_- have 2-D stable and unstable manifolds, respectively, it is possible that there exists a heteroclinic trajectory which goes from O_- to O_0 and located on the intersection of these manifolds, which persists under perturbations, as it is a bifurcation of codimension 0. If this is the case, then at the bifurcation parameter values there can exist heteroclinic loops which connect the equilibrium points of saddle type $O_0 \to O_- \to O_0$. These heteroclinic loops exist when the control parameters are taken from the bifurcation sets of codimension 2.

It is known that these bifurcation sets give rise to bifurcation sets of codimension 1 where the system has homoclinic orbits either from O_0 or O_- [20]. In this case the bifurcation sets of the homoclinicity are located on logarithmic spirals originating from the bifurcation points of the heteroclinic loops [21], [22].

V. Numerical and Theoretical Work on 1-D Map From Chua's Circuit

In this section, we give a brief summary of some recent work to construct and analyze 1-D maps from Chua's circuit numerically and theoretically. These results can be useful in confirming experimentally obtained results.

5.1. Calculating 1-D Map from Differential Equations

In the case of the period-doubling scenario to chaos, the two equilibrium states in the outer regions have a 1-D stable manifold and a 2-D unstable manifold. The stable eigenvalue is relatively large resulting in the trajectories being contracted onto the 2-D eigenplane of the unstable eigenvalues and the attractors tend to be "flat" in the outer regions, as was observed in experiments. For a suitable intersection plane in the outer region, the Poincaré map lives on a thin strip in the intersection plane. We can then approximate this by collapsing the map onto a 1-D line, resulting in a 1-D map. The approximate 1-D map in [23], [6] is obtained in this way. In general systems, finding the intersection of the trajectory with the Poincaré plane involves integrating the trajectory in small time steps until the trajectory is near the Poincaré plane, at which point an iterative scheme is used to find the intersection point [2]. In Chua's circuit, the vector field is piecewise linear and we can find an explicit formula for the trajectory in each linear region. However, finding the intersection of a trajectory with a Poincaré map still requires finding the solutions of transcendental equations. In [23], by choosing an appropriate 1-D line, the method used to compute the 1-D map does not require solving transcendental equations. Although this map is approximate, it has been useful in finding both stable and unstable periodic limit cycles, homoclinic and heteroclinic orbits and analyzing transitions to chaos.

5.2. Chua Maps and Chua Equations

The 1-D maps discussed above are obtained by making some simplifying assumptions on the 2-D Poincaré map.

By simplifying the *dynamics* of Chua's circuit, a class of 1-D maps can also be found which is similar to the 1-D map discussed earlier. For example, in [24], Brown starts with the vector field of Chua's circuit and shrinking the width of the middle region. When the middle region has zero width, a 2-region piecewise-linear vector field is obtained.[11] Since the vector field is odd-symmetric, the phase space is "folded" in half by associating the points $\boldsymbol{x}$ and $-\boldsymbol{x}$. Then the stable eigenvalue is increased to infinity, flattening all the dynamics to the unstable eigenplane. This 2-D system then gives rise to 1-D Poincaré maps, called Chua maps in [24], at $x = 0$. The map has the form $\boldsymbol{TF}$ where $\boldsymbol{F}$ is the reflection map with respect to a point on the eigenplane and $\boldsymbol{T}$ is a map which takes a point $\boldsymbol{x}$ as initial condition and follow the trajectory of the 2-D system until it hits the line x=0 using the intersection point as $\boldsymbol{T}(\boldsymbol{x})$.

In [25], a subset of these maps is studied in more detail and it was found that for certain parameter ranges, the Chua maps are unimodal with negative Schwarzian derivatives such as the logistic map. This implies that the dynamics will be similar to the logistic map.

5.3. Two-Parameter Renormalization Group Analysis

A renormalization group analysis was used by Feigenbaum [26] to explain the universal period-doubling scenario in the logistic map which is parameterized by one parameter. As mentioned before, a two-parameter analysis is required to understand the bifurcations in a map with more than one extrema. In [15] the 1-D map, which in the region of interest is bimodal, is studied when parameterized by two parameters. The critical points of doubly superstable period-2^n cycles[12] that form bifurcation points of codimension 2 are found, and a two-parameter renormalization group analysis is performed, which results in universal properties describing the self-similarity of bifurcation curves in the two-parameter plane. Our experimentally obtained description of the behavior in the two-parameter plane also shows self-similarity. See [15] and [27] for more details.

[11] Although the vector field is then discontinuous at the plane $x = 0$, this can be approximated as closely as needed by a C^∞ vector field.

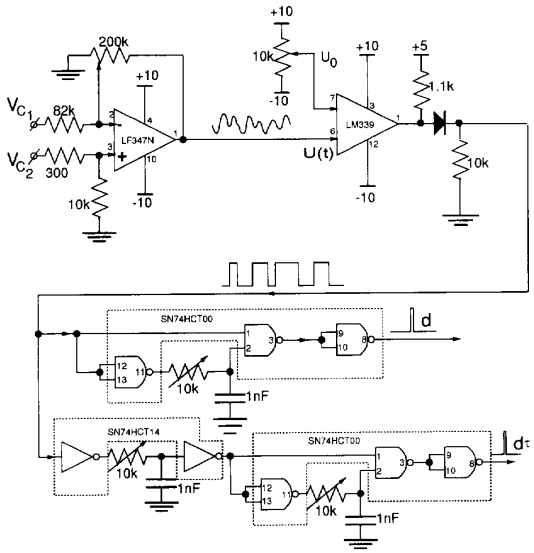

Fig. 22. Circuit schematic of Poincaré cross-sectoin circuit.

VI. Conclusions

We have seen how 1-D maps constructed from a continuous-time dynamical system, but experimentally and numerically, can provide much insight to the bifurcations occurring in the system. It can provide information about unstable periodic orbits and other unstable phenomena which a simple phase portrait analysis cannot provide. This technique of constructing 1-D maps from the trajectories can be applied to many other systems which are strongly dissipative.

Appendix
Implementation of the Poincaré Map Circuit and the 1-D Map Circuit

In this Appendix, we show the implementation details of the Poincaré map circuit and the 1-D map circuits shown in Fig. 6.

The circuit diagram of the Poincaré map circuit is shown in Fig. 22, and the circuit diagram of the 1-D map circuit is shown in Fig. 23.

[12] A superstable cycle is a cycle whose characteristic multiplier is smallest in absolute value, i.e., 0. Thus a superstable cycle must include an extremum in its orbit. A doubly superstable cycle has two extrema in its orbit.

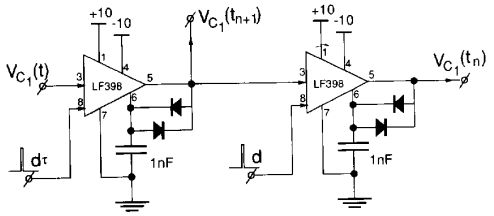

Fig. 23. Circuit schematic of 1-D map circuit.

In order to get the Poincaré cross-section of the attractors we use the adjustable plane in the phase space (v_{C_1}, v_{C_2}, i_L), see Fig. 7(a). The equation of the plane we use has the following form:

$$\alpha_1 v_{C_1} + \alpha_2 v_{C_2} = U_0. \tag{7}$$

From the Chua's circuit, the voltage $U_\Sigma(t) = \alpha_1 v_{C_1}(t) + \alpha_2 v_{C_2}(t)$ is calculated in the Poincaré cross-section circuit by the summing subcircuit. If the voltage $U_\Sigma(t)$ increases and crosses the value U_0 at t_n, where

$$\frac{dU_\Sigma(t)}{dt}|_{t=t_n} > 0$$

then the comparator subcircuit will output a rising edge. This is then used to generate a narrow pulse d at t_n. After a very small time delay τ the circuit generates the second pulse d_τ. We choose τ small enough so that the state of Chua's circuit remains almost constant during this time interval.

The pulse d_τ is used to "record" the points of the trajectory $(v_{C_1}(t), v_{C_2}(t))$ which is located on the plane (7). To show these points on the projections of the attractors we use the pulse d_τ to modulate the brightness of the beam in oscilloscope 1. This causes the points of the trajectories which are located in the intersection with the plane to appear as bright points against the rest of the trajectories.

If the parameters of the plane (α_1, α_2, and U_0) correspond to a transversal intersections of the plane with any trajectory of the attractor, then the plane can be used as a Poincaré plane. In the experiments we check the condition of transversal intersection by varying the parameters of the plane slightly. If all points of the attractor on the Poincaré cross section persist under small parameter variations then the plane has a transversal intersection with the trajectories of the attractor.

Fig. 23 shows two sample-and-hold circuits which are cascaded in series. The pulse d is used by the 1-D map circuit to load the value from the first sample-and-hold circuit onto a second sample-and-hold circuit. The pulse d_τ is then used to load a new value of v_{C_1} into the first sample-and-hold circuit. The value stored in the two sample-and-hold circuits corresponds to x and $f(x)$ where f is the 1-D map.

ACKNOWLEDGMENT

The authors would like to thank Prof. L. O. Chua for his support and useful comments.

REFERENCES

[1] R. L. Devaney, *An Introduction to Chaotic Dynamical Systems.* Benjamin/Cummings, 1986.

[2] T. Parker and L. O. Chua, *Practical Numerical Algorithms for Chaotic Systems.* New York: Springer-Verlag, 1989.

[3] S. Wiggins, "Introduction to applied nonlinear dynamical systems and chaos," in *Texts in Applied Mathematics.* New York: Springer-Verlag, 1990.

[4] A. Volkovskii and N. F. Rul'kov, "Use of one-dimensional mapping for an experimental study of the stochastic dynamics of an oscillator," *Sov. Tech. Phys. Lett.*, vol. 14, pp. 656–658, Aug. 1988.

[5] N. Rul'kov and A. R. Volkovskii, "Experimental analysis of 1-D map from Chua's circuit," in *Chua's Circuit: A Paradigm for Chaos* (R. N. Madan, Ed.). Singapore: World Scientific, 1993, pp. 580–590.

[6] L. O. Chua, M. Komuro, and T. Matsumoto, "The double scroll family, Parts I and II," *IEEE Trans. Circuits Syst.*, vol. CAS-33, pp. 1073–1118, 1986.

[7] M. Genot, "Applications of 1-D map from Chua's circuit: A pictorial guide," *J. Circuits Syst. Comput.*, vol. 3, pp. 375–409, June 1993.

[8] R. N. Madan, "Observing and learning chaotic phenomena from Chua's circuit," in *Proc. 35th Midwest Symp. Circuits Syst.*, 1992, pp. 736–745.

[9] R. Madan (Guest Editor), "Special issue on Chua's circuit: A paradigm for chaos," in *J. Circuit Syst. Comput.*, Mar. 1993, part I, vol. 3.

[10] P. Deregal, "Chua's oscillator: A zoo of attractors," *J. Circuits Syst. Comput.*, vol. 3, pp. 309–359, June 1993.

[11] M. P. Kennedy, "Robust op amp realization of Chua's circuit," *Frequenz*, vol. 46, no. 3–4, pp. 66–80, 1992.

[12] H. G. Schuster, *Deterministic Chaos, An Introduction* (2nd ed.). VCH, 1988.

[13] C. Grebogi, E. Ott, and J. A. Yorke, "Crises, sudden changes in chaotic attractors, and transient chaos," *Phys. D*, vol. 7, pp. 181–200, 1983.

[14] P. Gaspard, R. Kapral, and G. Nicolis, "Bifurcation phenomena near homoclinic systems: A two-parameter analysis," *J. Stat. Phys.*, vol. 35, pp. 697–727, 1984.

[15] A. P. Kuznetsov, S. P. Kuznetsov, I. R. Sataev, and L. O. Chua, "Two-parameter study of transition to chaos in Chua's circuit: renormalization group, universality and scaling," *Int. J. Bifurcation Chaos*, vol. 3, Aug. 1993.

[16] V. S. Afraimovich, *Internal Bifurcations and Crises of Attractors.* Moscow: Nauka, 1987, pp. 189–213 (in Russian).

[17] V. S. Afraimovich and L. P. Shilnikov, *Strange Attractors and Quasi-attractors.* New York: Pitman, 1983, pp. 1–34.

[18] L. A. Belyakov, "Bifurcation of systems with homoclinic curve of a saddle-focus with saddle value zero," *Math. Notes*, vol. 36, pp. 838–843, 1984.

[19] L. P. Shilnikov, "A contribution to the problem of the structure of an extended neighborhood of a rough equilibrium state of saddle-focus type," *Math. USSR Sbornik*, vol. 10, pp. 91–102, 1970.

[20] V. V. Bykov, "On bifurcations of dynamical systems close to those with separatrix contour containing a saddle-focus," Gorky State Univ., Gorky, Russia, 1980, pp. 44–72 (in Russian).

[21] P. Glendinning and C. Sparrow, "T-points: A codimension two heteroclinic bifurcation," *J. Stat. Phys.*, vol. 43, pp. 479–488, 1986.

[22] A. I. Khibnik, D. Roose, and L. O. Chua, "On periodic orbits and homoclinic bifurcations in Chua's circuit with a smooth nonlinearity," *Int. J. Bifurcation Chaos*, vol. 3, no. 2, pp. 363–384, 1993.

[23] M. Genot, "Applications of 1-D map from Chua's circuit: A pictorial guide," in *Chua's Circuit: A Paradigm for Chaos* (R. N. Madan, Ed.). Singapore: World Scientific, 1993, pp. 545–579.

[24] R. Brown, "From the Chua circuit to the generalized Chua map," *J. Circuits Syst. Comput.*, vol. 3, no. 1, pp. 11–32, 1993.

[25] M. Misiurewicz, "Unimodal interval maps obtained from the modified Chua's equations," *Int. J. Bifurcation Chaos*, vol. 3, pp. 323–332, Apr. 1993.

[26] M. J. Feigenbaum, "Universal behavior in nonlinear systems," *Los Alamos Sci.*, vol. 1, pp. 4–27, 1980 (reprinted in *Universality in Chaos* (P. Cvitanović, Ed.). Adam Hilger, 1984.

[27] R. S. MacKay and J. B. J. van Zeijts, "Period doubling for bimodal maps: A horseshoe for a renormalization operator," *Nonlinearity*, vol. 1, pp. 253–277, 1988.

Chai Wah Wu (S'88) received the B.S. degree in computer engineering and the B.A. degree in cognitive science from Lehigh University, Bethlehem, PA, in 1990 and the M.S. degree in electrical engineering from the University of California, Berkeley in 1991. He is currently working towards the Ph.D. degree in electrical engineering at the University of California, Berkeley.

His present technical interests include neural networks, nonlinear dynamics, chaos, and nonlinear signal processing.

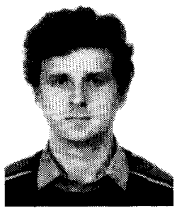

Nikolai F. Rul'kov was born in Russia. He received the B.S. degree in 1983 and the Ph.D. degree in 1991, both in physics and mathematics, from the University of Nizhny Novgorod, Russia.

Presently, he is a Senior Lecturer of the Radio Physics Department of the University of Nizhny Novgorod, Russia. In January 1991, July–September 1991, and July–October 1992, he was with the Facultad de Ciencias, U.N.E.D., Madrid, Spain, as a Visiting Scientist. From February to June 1993, he was on leave at the Department of Electrical Engineering and Computer Sciences, University of California, Berkeley. His research interests are in the areas of nonlinear dynamics, theory of synchronization, and chaotic oscillations in electronic systems.